

DIGITAL CONTROL OF MAGNETIC BEARINGS
SUPPORTING A MULTIMASS FLEXIBLE ROTOR

54-37
N93-27558
163484
P. 19

F. J. Keith, Research Associate (1)
R. D. Williams, Assistant Professor (1)
P. E. Allaire, Professor (2)
R. M. Schafer, Senior Research Engineer (3)

(1) Electrical Engineering Department
Thornton Hall
University of Virginia
Charlottesville, VA

(2) Mechanical and Aerospace Engineering Department
Thornton Hall
University of Virginia
Charlottesville, VA

(3) Tell Labs Research Center
Tell Labs, Inc.
Bldg. No. 2, Suite 101
3702 North Main St.
Mishawaka, Indiana

ABSTRACT

This paper considers the characteristics of magnetic bearings used to support a three mass flexible rotor operated at speeds up to 14,000 RPM. The magnetic components of the bearing are of a type reported in the literature previously, but the earlier analog controls have been replaced by digital ones. Analog-to-digital and digital-to-analog converters and digital control software were installed in an AT&T PC. This PC-based digital controller was used to operate one of the magnetic bearings on the test rig. Basic proportional-derivative control was applied to the bearings, and the bearing stiffness and damping characteristics were evaluated. Particular attention is paid to the frequency dependent behavior of the stiffness and damping properties, and comparisons are made between the actual controllers and ideal proportional-derivative control.

INTRODUCTION

This paper discusses the development of digital controls for magnetic bearings. An analog controlled magnetic bearing developed by the Rotating Machinery and Controls Laboratory at the University of Virginia has been described in several articles [1-4]. A PC-based digital controller has been implemented for the same magnetic components and flexible rotor.

Magnetic bearings are coming into increasing commercial use in rotating machinery. Uses include industrial applications such as compressors, turbines and pumps, and space related applications such as momentum wheels, turbomolecular pumps and attitude control devices. Magnetic suspension devices can also be used in other applications such as wind tunnels. A full literature review for all magnetic bearings is beyond the scope of this paper - the emphasis here is on digital controls for magnetic bearings.

Single-axis digital control has been reported by several authors. Hisatani, et al. [5] described the magnetic support of a 1 kg vertical rotor supported by a digitally controlled axial active magnetic bearing. They noted that the particular digital control algorithm used was successful but not quite as good as the corresponding analog one. Carmichael, et al. [6] reported the use of digital controls in a single axis vertical support for a 1 in diameter ball. Scudiere, et al. [7] employed a microprocessor based digital control system to support small steel spheres and small vertical rotors with masses up to 90 grams.

52 INTERNATIONAL BRAND

Digital control of magnetic suspension and balance systems for wind tunnels has been described by Britcher, et al. [8,9]. Like magnetic bearings, these suspension systems are inherently unstable. Digital controls provide the means to stabilize them with a much greater degree of flexibility than analog controls. The system employed for the wind tunnels is much more complicated than the single axis control systems indicated above because many axes are involved. A PDP 11/84 minicomputer was chosen for implementing the digital controller.

A theoretical treatment of digital control for radial bearings was given by Schweitzer and Ulbrich [10] but not tested. Bleuler and Schweitzer [11] analyzed the use of decentralized control for radial magnetic bearings as preparation for the application of microprocessor-based digital controls. Gondhalekar and Holmes [12] developed a magnetic bearing for control of transmission shaft vibrations. Traxler, et al. [13] described a radial bearing using a microprocessor-based digital control. The microprocessor software consisted of a main program and an interrupt handler. Also, a magnetic bearing with digital control has been developed utilizing a rotational interrupt [14]. The system was employed on a single-mass rotor supported at one end. Orbit and other vibration plots indicated successful operation of the bearing.

The purpose of this paper is to demonstrate the relationships between the analog and digital controllers used to stabilize the magnetic bearing and the resulting bearing stiffness and damping properties. Earlier work on this test rig [ref. 1] has shown the effect of control algorithms similar to those reported here; this work will extend the earlier work, with particular attention paid to the frequency dependence of the magnetic bearing dynamic properties. Comparison is made between the actual controllers and equivalent ideal controllers which do not exhibit this frequency dependence. Both analog and digital control systems are shown to be effective for controlling vibrations of the test rotor and for exerting a great deal of control over the dynamic properties of the magnetic bearing.

NOMENCLATURE

A/D	Analog-to-digital convertor	K_r	Analog derivative feedback gain constant
A_g	area of air gap perpendicular to magnetic flux	K_s	Position probe sensitivity
C	Capacitance	K_t	Loop gain for analog PD controller
$C_{eq}(\omega)$	Frequency dependent damping characteristic of magnetic bearing	m	Mass
D/A	Digital-to-analog converter (see ZOH)	N	Number of coil turns per pole pair
D(z)	Digital control algorithm	PD	Proportional-derivative
F	Force	R	Resistance
F_{ext}	Externally applied force	s	Laplace variable, $s = j\omega$
g	length of the air gap	SR	Sampling rate
G	Nominal undeflected gap length ($y=0$)	T	Sampling period
G(s)	Continuous domain transfer function	W	Weight
I_{bx}, I_{by}	Bias current in magnet coil	z	Z-transform variable, $z = e^{sT}$
i_{px}, i_{py}	Perturbation current in magnet coil	ZOH	Zero-order-hold device (see D/A)
K_a	Power amplifier transconductance	β	sensitivity of the air gap to shaft displacement: $\frac{\partial g}{\partial x}$
$K_{A/D}$	A/D converter gain (counts/volt)	μ_0	Permeability of free space
$K_{D/A}$	D/A converter gain (volts/count)	μ_r	Relative permeability
K_d	First derivative feedback gain constant	μ	Permeability, $\mu = \mu_0 \mu_r$
$K_{eq}(\omega)$	Frequency dependent stiffness characteristic of magnetic bearing	τ_a	Power amplifier LPF time constant
K_g	Analog proportional feedback gain constant	$\tau_{A/D}$	A/D conversion time
K_{ix}, K_{iy}	Actuator gain of magnetic bearing in x and y directions	τ_{comp}	Computation time of digital control algorithm
K_{myy}, K_{mxx}	Magnetic position stiffness (i, j = x or y)	τ_{in}	Input LPF time constant (digital controller)
K_p	Proportional feedback gain constant	τ_{out}	Output LPF time constant (different for analog and digital controllers)
K_{pert}	Perturbation input gain of power amplifier	τ_s	Position probe LPF time constant
		Φ	Magnetic Flux
		ω	Frequency (rad/sec)

SECTION 1 - Description of Magnetic Bearing

The magnetic bearings used to support the flexible rotor in this work consist of four electromagnets arranged radially around the shaft as shown in Figure 1. Varying the currents in the magnet coils determines the forces on the bearing journal (the magnetic laminations), thus determining the static and dynamic properties of the magnetic bearing. Maslen, et al. [ref. 15] present the governing equation for a bearing of this type, which for small displacements about $y = 0$, can be linearized as

$$F_y = K_{iy}i_{py} - K_{myy}y \quad (1)$$

where

$$K_{iy} = \frac{\mu_0 A_g N^2 I_{by} \beta}{G^2} \quad (2)$$

and

$$K_{myy} = -\frac{\mu_0 A_g N^2 I_{by}^2 \beta^2}{G^3} \quad (3)$$

K_{iy} and K_{myy} are referred to as the *actuator gain* and the *position stiffness*, respectively.

SECTION 2 - Controller Configuration and Block Diagram

We now wish to incorporate these force relationships (K_{myy} and K_{iy}) into a block diagram configuration of the magnetic bearing. The equation of motion for the bearing journal is (see Figure 2):

$$f_{ext} = m\ddot{y} + K_{myy}y + K_{iy}i_{py} \quad (4)$$

if we assume that i_{py_0} is chosen so that $K_{iy}i_{py_0} = -W$, and that i_{py} has been redefined about the operating point i_{py_0} (allowed here since K_{iy} is a linear function of i_{py}).

Taking the Laplace transform gives the steady state solution:

$$F_{ext} = (ms^2 + K_{myy})Y(s) + K_{iy}I_{py}(s) \quad (5)$$

Re-arranging this equation gives:

$$\frac{Y(s)}{F_{ext} - K_{iy}I_{py}(s)} = \frac{1}{ms^2 + K_{myy}} \quad (6)$$

where $F_{ext} - K_{iy}I_{py}(s)$ represents the total exogenous force applied to the rotor (see Figure 3).

Inspection of the characteristic equation of this transfer function reveals that the system is open-loop unstable, since $K_{myy} < 0$. Thus, we must employ active feedback control to stabilize the system. Designating the controller as $G(s)$, a controller which relates rotor position y (or x) to actuator current i_{py} (or i_{px}), we have the configuration shown in Figure 4.

The CLTF (closed loop transfer function) for the magnetic bearing system with this feedback is

$$\frac{Y(s)}{F_{ext}} = \frac{1}{ms^2 + K_{myy} + K_{iy}G(s)}, \quad K_{myy} < 0 \quad (7)$$

which can also be written:

$$Y(s)[ms^2 + K_{myy} + K_{iy}G(s)] = F_{ext} \quad (8)$$

We are interested in the relationships between the controller $G(s)$ and the stiffness and damping properties of the magnetic bearing. For the single degree-of-freedom (SDOF) bearing model shown in Figure 5, the equation of motion is:

$$Y(s)[ms^2 + C_b s + K_b] = F_{ext} \quad (9)$$

Thus, we wish to relate the SDOF stiffness and damping coefficients K_b and C_b to the feedback controller $G(s)$.

This relationship must be made with care, however. It is important to realize that, because the forces generated by a magnetic bearing are a function of, among other things, a frequency dependent transfer function, $G(s)$, the stiffness and damping properties experienced by the bearing journal (and hence the rotor) will be different for different radial excitation frequencies. We introduce frequency dependent stiffness and damping coefficients, $K_{eq}(\omega)$ and $C_{eq}(\omega)$, to replace terms K_b and C_b for realizable controllers. It is important to note that ω does not refer to the rotational frequency of the rotor, but rather the radial vibration frequency of the bearing journal.

Now, we combine equation (8) and equation (9) as follows:

$$Y(s)[ms^2 + K_{myy} + K_{iy}G(s)] = Y(s)[ms^2 + C_{eq}(\omega)s + K_{eq}(\omega)] \quad (10)$$

Cancelling like terms, substituting $s = j\omega$ and separating real and imaginary parts of the equations gives:

$$K_{eq}(\omega) = K_{myy} + K_{iy}\text{Re}\{G(j\omega)\} \quad (11)$$

$$C_{eq}(\omega) = K_{iy} \frac{\text{Im}\{G(j\omega)\}}{\omega} \quad (12)$$

Thus, for the SDOF model of the magnetic bearing/rotor system, we have a relationship between the bearing stiffness and damping characteristics and the controller transfer function.

SECTION 3 - Analog implementation of PD control

The Routh criterion [ref. 16] dictates that the system described by equation (7) is open-loop unstable. Stabilization requires that both proportional and derivative terms be present in $G(s)$, the controller transfer function. Without considering stability, earlier works have demonstrated the utility of derivative feedback for reducing vibration in rotating systems [ref. 17]. This suggests a transfer function of the form:

$$G(s) = K_p + K_d s \quad (13)$$

Combining with the expressions for $K_{eq}(\omega)$ and $C_{eq}(\omega)$ (equations 11 and 12) leads to:

$$K_{eq}(\omega) = K_{myy} + K_{iy}K_p \quad (14)$$

$$C_{eq}(\omega) = K_{iy}K_d \quad (15)$$

In other words, the bearing stiffness is a linear function of K_p (the proportional feedback coefficient), and the bearing damping is a linear function of K_d (the derivative feedback coefficient).

As it turns out, this controller cannot be implemented perfectly. In particular, an infinite bandwidth differentiator will exacerbate the effects of any extraneous noise in the system; high frequency poles must be included in the actual design to avoid this problem. Also, the proximity probes and power amplifiers employed in a real control system will have finite bandwidth and will introduce additional poles into the controller transfer function, $G(s)$. The analog controller reported in this work is represented by:

$$G(s) = \frac{0.01K_s K_r K_d [R_1 C (0.1K_r)s + K_g (1 + RCs)(1 + R_1 C_1 s)]}{(1 + \tau_s s)(1 + RCs)(1 + R_1 C_1 s)(1 + \tau_{out} s)(1 + \tau_a s)} \quad (16)$$

Figure 6 shows a block diagram of this controller. Note that for the actual analog controller, the proportional feedback gain coefficient is denoted by K_g and the derivative feedback gain coefficient is written K_r . Values for the various system parameters described in this paper are presented in Appendix A.

SECTION 4 - Digital Implementation of PD Control

The digital implementation of proportional-derivative feedback is quite similar to the analog one. The proximity probes and power amplifier used with the analog controller are retained in the digital design; after all, the interface between any control system and a physical device must ultimately be analog in nature. The difference between the analog and digital systems lies mainly with the core elements of the system: while the analog controller employs resistors and capacitors to realize continuous differential equations, the transfer function of the digital controller results from repeated evaluation of a difference equation. The periodic rate at which the computer evaluates this difference equation is called the *sampling rate*.

Figure 7 is a block diagram of the digital controller. As mentioned earlier, it shares many features with its analog counterpart - namely, the proximity probe interface and the power amplifier. There are, however, notable differences. Before a signal can be processed by a difference equation, it must be converted to a numerical value, thus requiring the presence of an Analog-to-Digital converter between the position signal input and the digital computer. Likewise, the periodic stream of numbers generated by successive solutions of the difference equations must be converted back to analog voltage signals by a Digital-to-Analog converter prior to power amplification.

Proportional-derivative control is achieved digitally by converting the analog PD algorithm [equation (13)] to its discrete equivalent. The approximation used here is the backwards difference rule for approximating the Laplace variable s . The resulting equivalence is

$$s = \frac{(z - 1)}{Tz} \quad (17)$$

where T is the sampling period (inverse of sampling rate) and $z = e^{sT}$. Substituting for s in equation (13) and taking the inverse z -transform yields the difference equation:

$$c_n = K_p r_n + \frac{K_d}{T} (r_n - r_{n-1}) \quad (18)$$

where r_n and c_n are points in the input and output data streams of the digital computer, respectively. Note that the backwards difference rule approximates the derivative of the incoming signal by determining the slope of a straight line intersecting the most recent two data points in the input stream. Detailed discussion of z -transform theory and other approximation rules can be found in Franklin & Powell [ref. 18].

The digital controller discussed in this paper was implemented on an AT&T PC6300 personal computer (IBM PC/XT compatible). Even though this computer has an 8 MHz system clock and is outfitted with the Intel 8087 math co-processor, its computational abilities are somewhat limited. Thus, in order to achieve the highest possible sampling rate for the controller, the software that actually performs the difference equation calculations is written in 8086/8087 assembly language. Admittedly, assembly language programming is a somewhat tedious task; unfortunately, high-level languages (such as Pascal or Fortran) generate machine-level programs that are much longer, and hence much slower to execute, than an equivalent assembly language program. Given the computational constraints imposed by the PC, assembly language implementation of the digital PD algorithm is the only reasonable approach. The maximum sampling rate achieved for this software is 2.86 kHz ($T = 350 \mu\text{S}$).

SECTION 5 - Frequency Dependence of Stiffness and Damping Characteristics

In Section 3 it was shown that implementation of ideal PD control produced a system in which the stiffness and damping properties of the magnetic bearing could be determined by choice of two controller parameters K_p and K_d . In practice, however, such an ideal controller cannot be built. Thus, we investigate the effects of finite-bandwidth controllers on the bearing's stiffness and damping properties [$K_{eq}(\omega)$ and $C_{eq}(\omega)$].

Figures 8A, 8B, 9A and 9B present calculated values of $K_{eq}(\omega)$ and $C_{eq}(\omega)$ for the analog controller as functions of the radial excitation frequency encountered at the bearing location. The ideal curves represent the expected behavior of the ideal PD controller postulated in equation (13); the actual curves show the calculated stiffness and damping properties of the controller actually tested for this work [equation (16)]. Note that at low frequencies, the ideal and actual controllers behave quite similarly. As the excitation frequency is increased, however, the high frequency limitations of the actual controller are no longer negligible, and their presence starts to degrade the performance of the magnetic bearing. In addition, the independent behavior of the ideal stiffness and damping properties as functions of K_p and K_d is not fully realized with the actual controller: varying K_p has a slight effect on the damping curve (Figure 8B), and changes in K_d can be seen in the stiffness properties (Figure 9A).

Similar stiffness and damping curves are presented in Figures 10A, 10B, 11A and 11B for the digital PD controller, although for these curves, definition of an 'ideal' controller is a somewhat arbitrary task. In general, higher sampling rates result in improved controller performance, so our ideal digital controller is defined as one which has a sampling rate of 1 MHz (roughly 400 times faster than the actual digital controller presented here). Once again, the bandwidth limitations of the actual controller are clear: bearing performance is degraded at high

frequencies, and the relationships between the controller parameters (K_p , K_d) and the stiffness and damping properties are not completely independent.

While there is clearly some deviation from ideal controller behavior at high frequencies, we note that both the analog and digital controllers behave in a very similar fashion, in spite of the fact that the resistor-capacitor network that makes up the analog control system is obviously quite different from the regularly re-evaluated difference equation in the digital control system. This similarity results from the imperfect high frequency derivative calculations performed by both controllers: analog differentiator performance is limited by the presence of the high frequency poles mentioned earlier, and the straight-line derivative approximation used in the digital control system becomes progressively less accurate as the input signal frequency is increased. Note that a faster sampling rate would improve the high frequency performance of the digital controller, as increasing the roll-off points of the poles associated with the analog differentiator would increase the usable bandwidth of the analog controller.

SECTION 6 - Experimental Results

The test rig used to evaluate bearing performance is shown in Figure 12. Three shaft masses were mounted on the 1/2 inch diameter flexible shaft as shown; the magnetic bearing journals each weigh 5.12 N (1.15 lb), and the center mass weighs 7.88 N (1.77 lb). For all of the experimental results gathered, the inboard bearing was controlled by the analog controller with parameter settings $K_g=2.0$ and $K_r=4.0$. Two sets of tests were performed: the stiffness of the bearing was varied while the damping was held constant, and the damping was adjusted while the stiffness remained unchanged. These tests were run for both the analog and digital PD controllers, and the results presented represent the vertical vibration response at the outboard bearing (outboard horizontal responses were very similar to the vertical results).

The effect of varying the proportional feedback (stiffness) for both controllers is presented in Figures 13A and 13B. The curves represent the vertical amplitude response of the rotor as observed at the outboard bearing (similar results were obtained for the inboard bearing and are not presented here). The curves clearly indicate that bearing stiffness is increasing with greater amounts of proportional feedback: for frequencies below the first critical speed (about 1800 RPM), the amplitude of vibration is reduced as the proportional feedback is increased.

At higher frequencies, there are two other peaks (critical speeds) at about 3700 RPM and 5500 RPM. Changes in the bearing stiffness have little effect on the second critical because the rotor has a conical mode shape for this critical. It is nearly a rigid body mode shape with the ends rotating 180 degrees out of phase, and the center is a node point, so the bearing damping effectively keeps this peak small. The third critical is quite different. It is a bending mode with the end masses (bearing magnetic laminated disks) out of phase with the center mass. Apparently, increasing the bearing stiffness increases the peak vibration level, a result which is counter to intuition. What seems to be happening is that the magnetic force is applied at the disk location and probably does decrease the shaft motion at the bearing location, but the sensor is located a small distance away from the disk center and reports an apparent increase in the peak vibration level. Thus, the measured amplitude of motion increases with increasing K_p .

Rotor responses in the presence of various amounts of bearing damping are presented in Figures 14A and 14B. For both the analog and digital controllers, the measured results confirm the expectations for this test: as the bearing damping is increased by increasing the derivative feedback, the peak amplitude responses at the critical speeds are significantly reduced, and the critical frequencies themselves are moved to higher frequencies (this last effect is most noticeable at the third critical speed, which varies from 4600 RPM to 5600 RPM as K_d is increased from 2.0 to 3.5 via the digital controller).

SECTION 7 - Conclusions

A PC-based digital control system has been designed and tested for controlling a radial magnetic journal bearing. Implementation of a proportional-derivative control algorithm on the digital computer has been shown to yield similar results to those obtained with an analog PD controller. For both controllers, varying the proportional gain coefficient altered the stiffness of the magnetic bearing, and varying the derivative gain changed the effective damping of the magnetic bearing.

The frequency dependent nature of the effective stiffness and damping properties of the magnetic bearing has been investigated. High frequency poles present in the actual analog controller introduced phase-lag into the control signal, and degraded operation of the magnetic bearing system at higher frequencies. Computational delays and zero-order-hold effects in the digital controller were seen to have effects similar to those produced by the high frequency poles present in the analog system.

Both the analog and digital controllers were effective at altering the dynamic properties of the bearing under test. Judicious choice of the controller parameters (K_g & K_r for the analog controller, K_p & K_d for the digital controller) allows significant alteration of the vibration amplitudes and critical speeds of the rotor system.

The introduction of digital control into a magnetic bearing system offers the potential for evaluation and testing of algorithms much more complex than would be possible with an analog controller. For example, addition of an integrator to the controller creates a system which rejects static loads on the rotor. This addition is a somewhat tedious chore with an analog system, but with a digital controller it can be accomplished by merely installing a different software program on the computer. Also, complex digital control algorithms which can 'shape' the $K_{eq}(\omega)$ and $C_{eq}(\omega)$ curve to meet certain specifications can be developed and tested. Analog realization of such algorithms would be very difficult, if it were even possible. Thus, digital control provides bearing designers a flexible tool with which they can design bearings exhibiting dynamic properties unlike those of any passive bearings.

The authors would like to thank the Center for Innovative Technology of the Commonwealth of Virginia and the Army Research Office for partial support of this project.

This material is based upon work supported under a National Science Foundation Graduate Fellowship. Any opinions, findings, conclusions or recommendations expressed in this publication are those of the authors and do not necessarily reflect the views of the National Science Foundation.

REFERENCES

1. Humphris, R. R., Kelm, R. D., Lewis, D. W., and Allaire, P. E., "Effect of Control Algorithms on Magnetic Journal Bearing Properties," *Journal of Engineering for Gas Turbines and Power*, Trans. ASME, Vol. 108, October, 1986, pp. 624-632.
2. Allaire, P. E., Humphris, R. R., Kasarda, M. E. F., and Koolman, M. I., "Magnetic Bearing/Damper Effects on Unbalance Response of Flexible Rotors," *Proc. AIAA Conference*, Philadelphia, PA., August 10-14, 1987.
3. Allaire, P. E., Humphris, R. R., and Barrett, L. E., "Critical Speeds and Unbalance Response of a Flexible Rotor in Magnetic Bearings," *Proceedings of European Turbomachinery Symposium*, October 27-28, 1986.
4. Allaire, P. E., Humphris, R. R., and Imlach, J., "Vibration Control of Flexible Rotors with Magnetic Bearings Supports," *AFOSR/ARO Conference, Non-Linear Vibrations, Stability and Dynamics of Structures and Mechanisms*, Virginia Tech, Blacksburg, Virginia, March 23-25, 1987.
5. Histani, M., Inoue, Y. and Mitsui, J., "Development of Digitally Controlled Magnetic Bearing," *Bulletin of JSME*, Vol. 29, No. 247, January 1986, pp. 214-220.
6. Carmichael, A. T., Hinchliffe, S., Murgatroyd, P. N. and Williams, I. D., "Magnetic Suspension Systems with Digital Controllers," *Review of Scientific Instruments*, Vol. 58, No. 8, August 1986, pp. 1611-1615.
7. Scudiere, M. B., Willems, R. A. and Gilles, G. T., "Digital Controller for a Magnetic Suspension System," *Review of Scientific Instruments*, Vol. 58, No. 8, August 1986, pp. 1616-1626.
8. Britcher, C. P., "Progress Toward Magnetic Suspension and Balance Systems for Large Wind Tunnels," *AIAA Journal of Aircraft*, April, 1985.

9. Britcher, C. P., Goodyer, M. J., Eskins, J., Parker, D. and Halford, R. J., " Digital Control of Wind Tunnel Magnetic Suspension and Balance Systems," Proceedings of the ICIASF Record - International Conference on Instrumentation in Aerospace Simulation Facilities, Williamsburg, VA, June 22-25, 1987.
10. Schweitzer, G. and Ulbrich, H., "Magnetic Bearings - A Novel Type of Suspension," Institution of Mechanical Engineers, Second International Conference on Vibrations in Rotating Machinery, Cambridge, September 1980, Paper C 273/80.
11. Blueler, H., Schweitzer, G., "Dynamics of a Magnetically Suspended Rotor With Decentralized Control," First IASTED International Symposium on Applied Control and Identification, Copenhagen, Denmark, June 28-July 1, 1983, pp. 17-22.
12. Gondhalekar, V. and Holmes, R., "Design of an Electromagnetic Bearing for the Vibration control of a Flexible Transmission Shaft," Rotor Dynamic Instability Problems in High Performance Turbomachinery, Texas A&M University, May 1984.
13. Traxler, A., Meyer, F. and Murbach, H. P., "Fast Digital Control of a Magnetic Bearing with a Microprocessor," International Kongress Mikroelektronik, Munich, November 13-15, 1984.
14. Nagai, B., Okada, Y., and Shimane, T., "Digital Control of Magnetic Bearing with Rotationally Synchronized Interrupt," Ibaraki University.
15. Maslen, E., Hermann, P., Scott, M., and Humphris, R. R., "Practical Limits to the Performance of Magnetic Bearings: Peak Force, Slew Rate and Displacement Sensitivity.," Presented at the NASA Workshop on Magnetic Suspension Technology, February 2-4, 1988, NASA CP- 3202, 1993.
16. D'Azzo, J. J., and Houpis, C. H., *Linear Control System Analysis and Design*, McGraw-Hill Book Company, 1981.
17. Allaire, P. E., Lewis, D. W., and Knight, J. D., "Active Vibration Control of a Single Mass Rotor on Flexible Supports," *Journal of the Franklin Institute*, Vol. 315, No. 3, 1983, pp. 211-22.
18. Franklin, G. F., and Powell, J. D., *Digital Control of Dynamic Systems*, Addison-Wesley Publishing, 1981.

APPENDIX A - Parameters for Magnetic Bearing Control System

A_g :	0.53 in ² (3.42 cm ²)	N :	1840 turns per pole pair
G :	39 mils (0.99 mm)	RC :	220 μ S (720 Hz)
I_{bx}, I_{by} :	250 mA	R_1C :	22 mS
K_a :	0.5 A/V	R_1C_1 :	100 μ S (1.6 kHz)
$K_{A/D}$:	4096 counts/10 volts	τ_a :	100 μ S (1.6 kHz)
$K_{D/A}$:	5 volts/4096 counts	$\tau_{A/D}$:	25 μ S
K_d :	0 to 10	τ_{comp} :	175 μ S for PD controller
K_g :	0 to 10	τ_{in} :	10.3 μ S (15 kHz)
K_p :	0 to 10	τ_{out} (analog):	47 μ S (3.4 kHz)
K_{pert} :	0.11 A/V	τ_{out} (digital):	155 μ S (1.0 kHz)
K_r :	0 to 10	τ_s :	56 μ S (2.8 kHz)
K_s :	200 mV/mil (7.87 V/mm)		
K_t :	0 to 10		

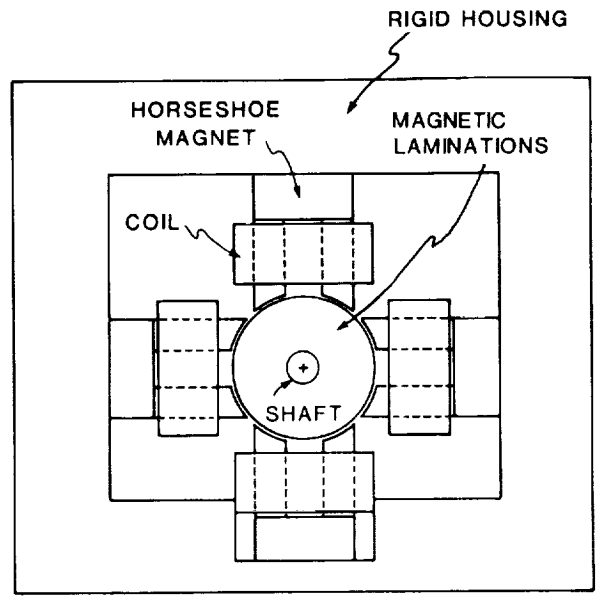


Figure 1 - Magnetic Bearing Configuration

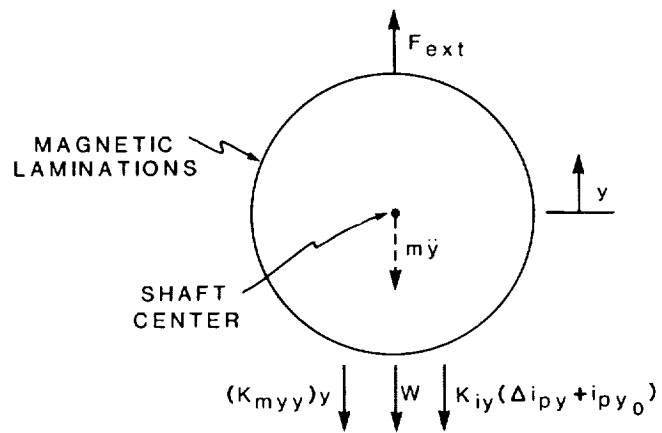


Figure 2 - Forces on Magnetic Bearing Journal

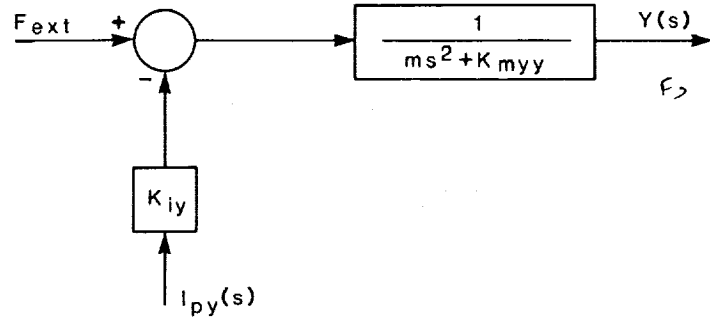


Figure 3 - Open-loop Magnetic Bearing System

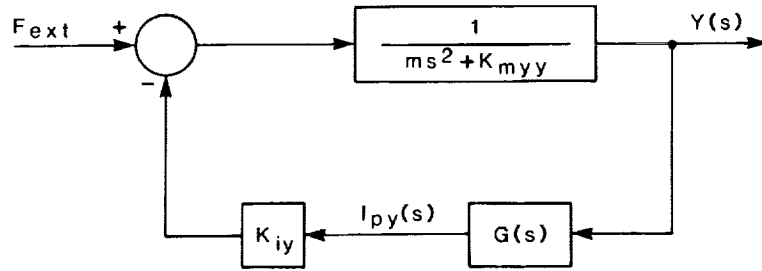


Figure 4 - Closed-loop Magnetic Bearing System

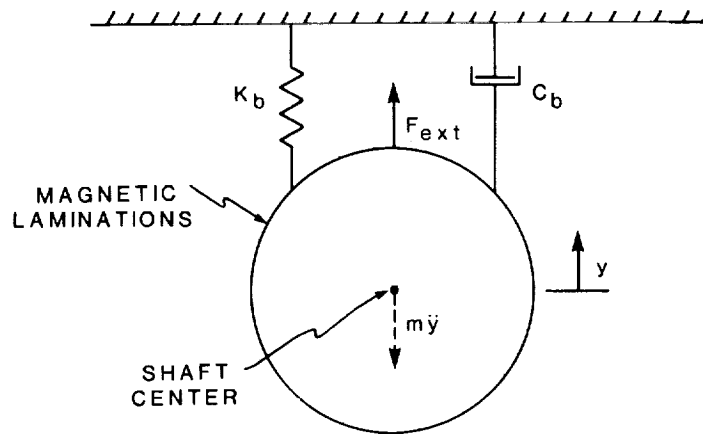


Figure 5 - Single Degree-of-Freedom Bearing Model

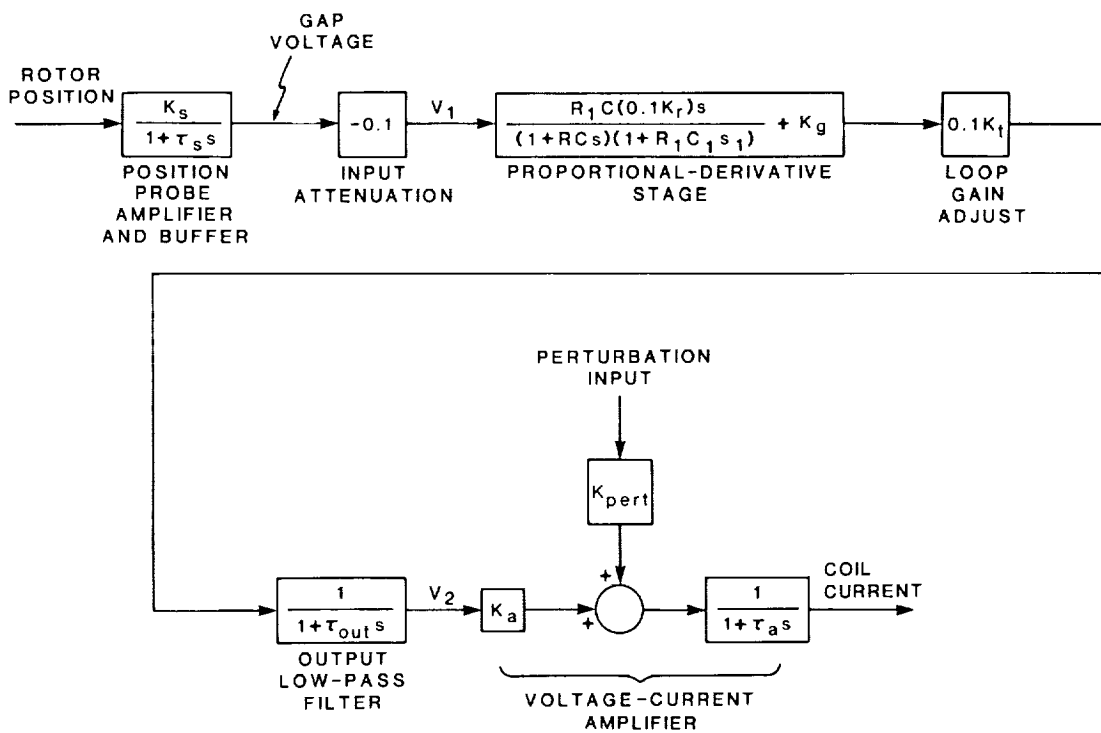


Figure 6 - Analog Controller (Block Diagram)

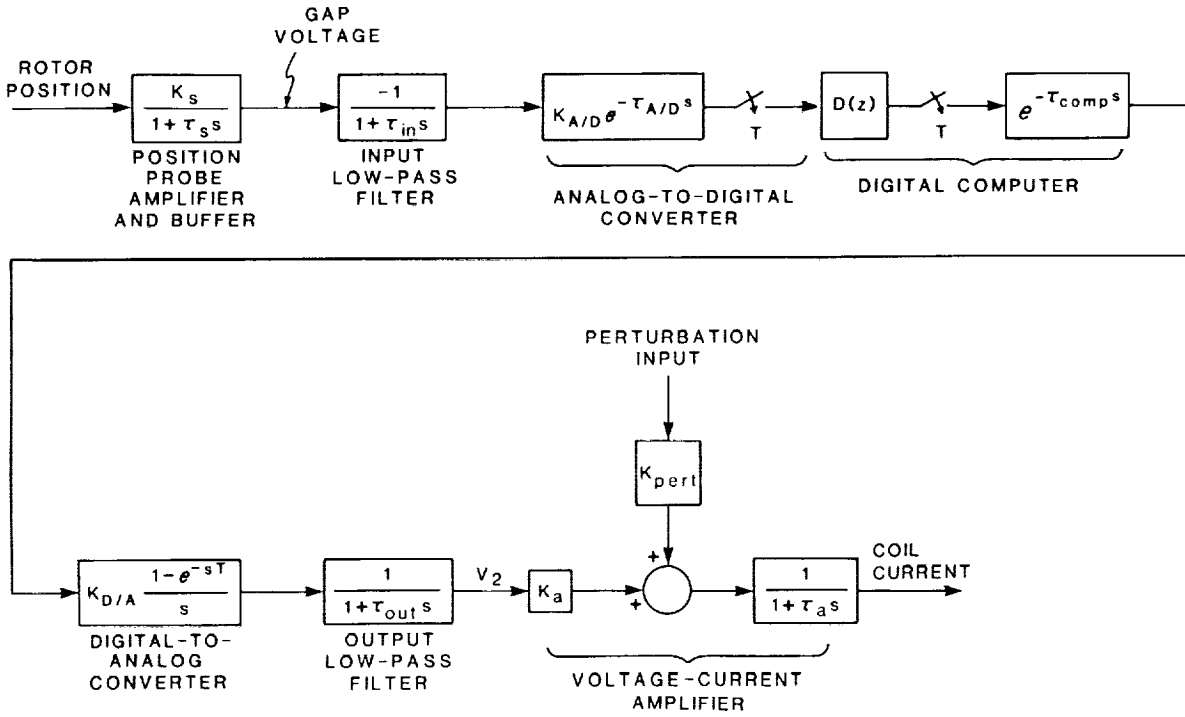
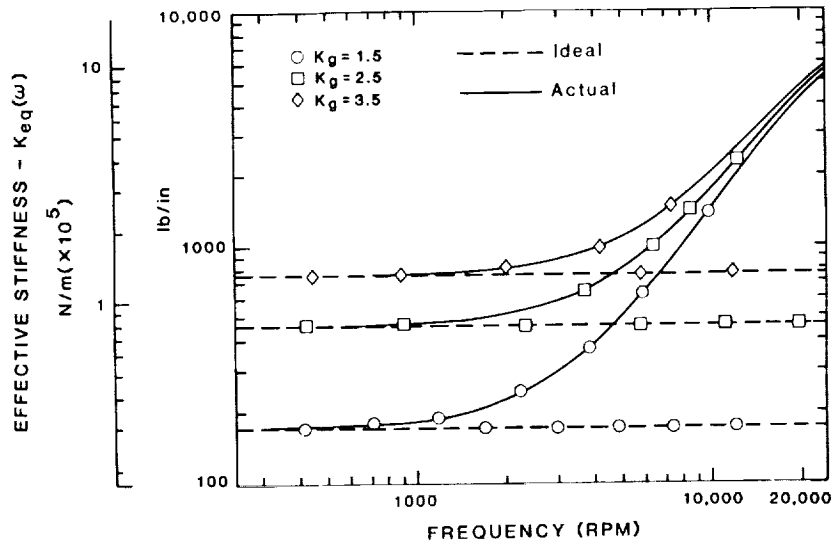
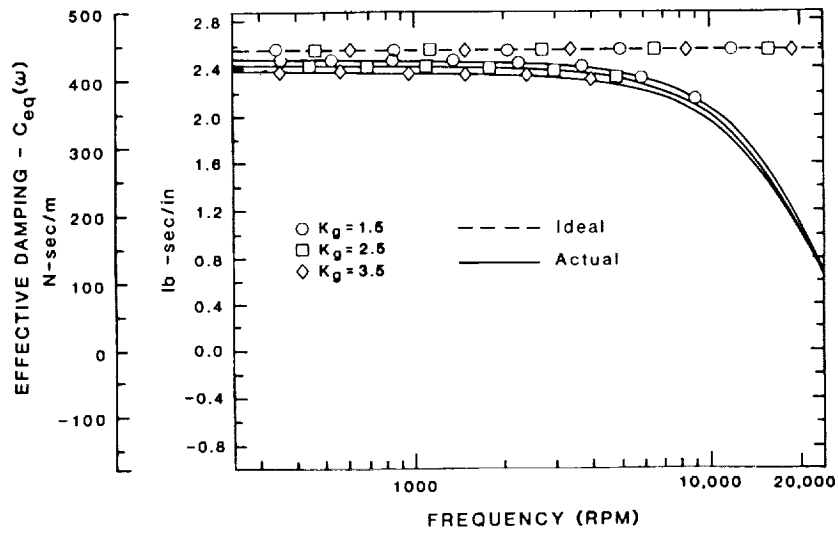


Figure 7 - Digital Controller (Block Diagram)

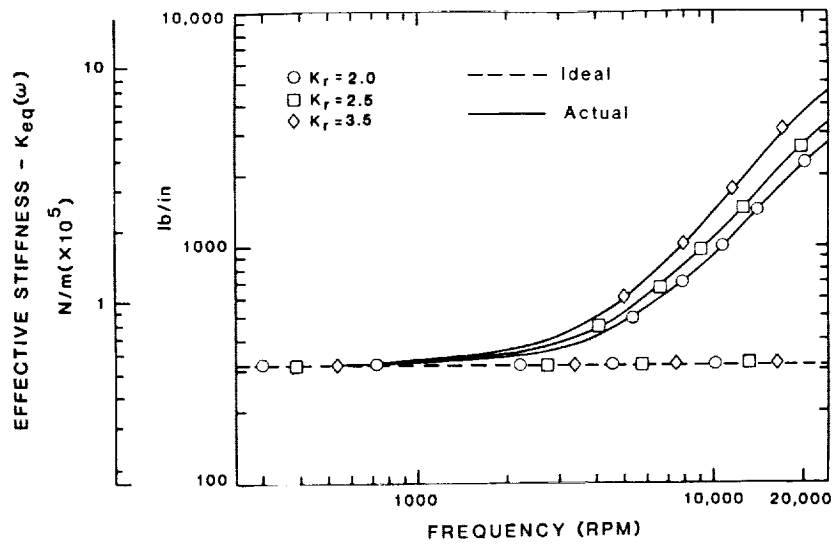


(A)

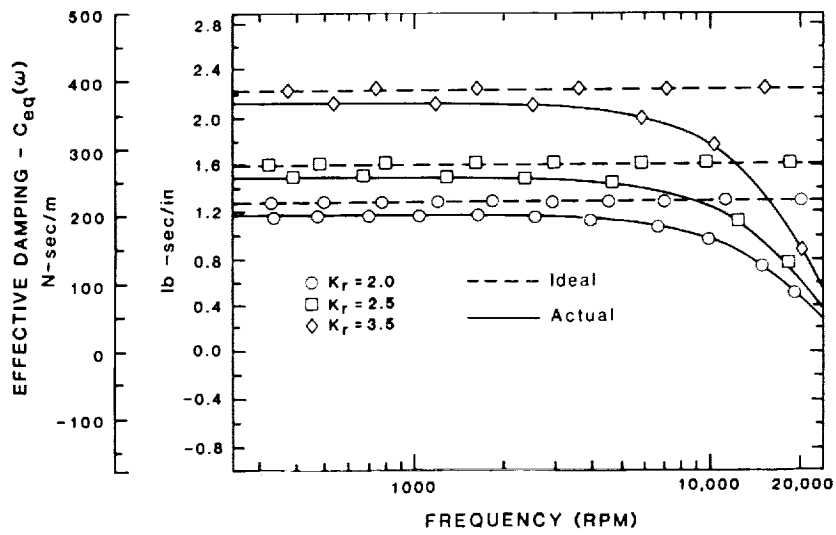


(B)

Figures 8A & 8B - $K_{eq}(\omega)$ and $C_{eq}(\omega)$
Varying Proportional Feedback (Analog)

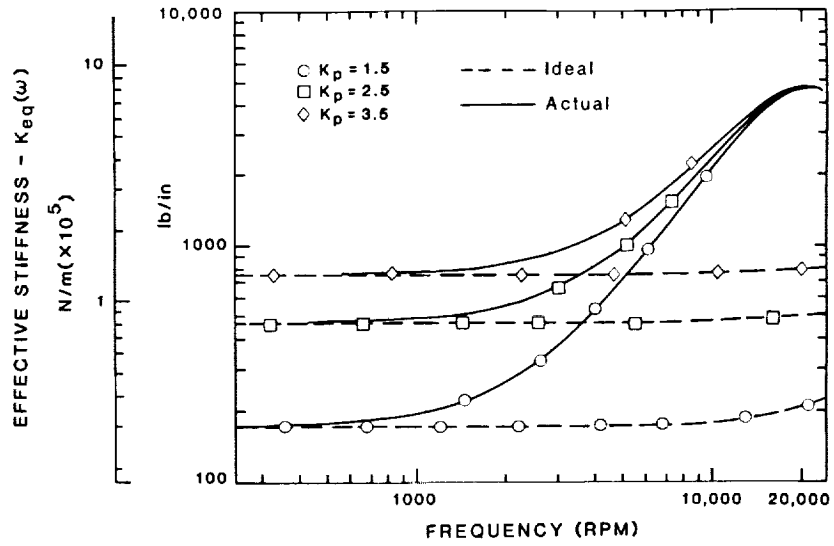


(A)

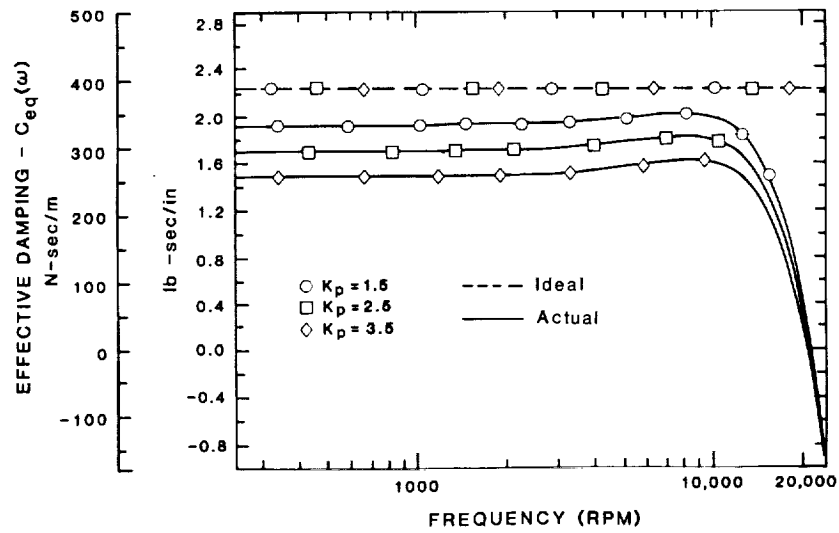


(B)

Figures 9A & 9B - $K_{eq}(\omega)$ and $C_{eq}(\omega)$
Varying Derivative Feedback (Analog)

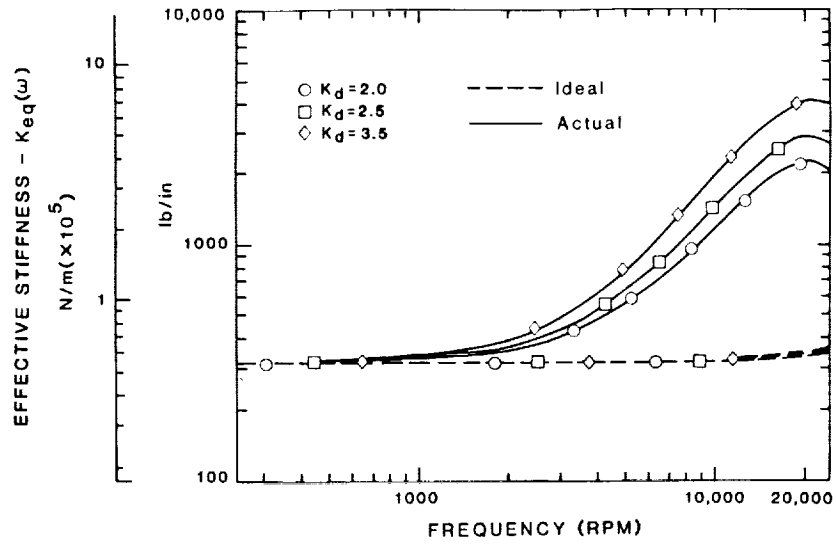


(A)

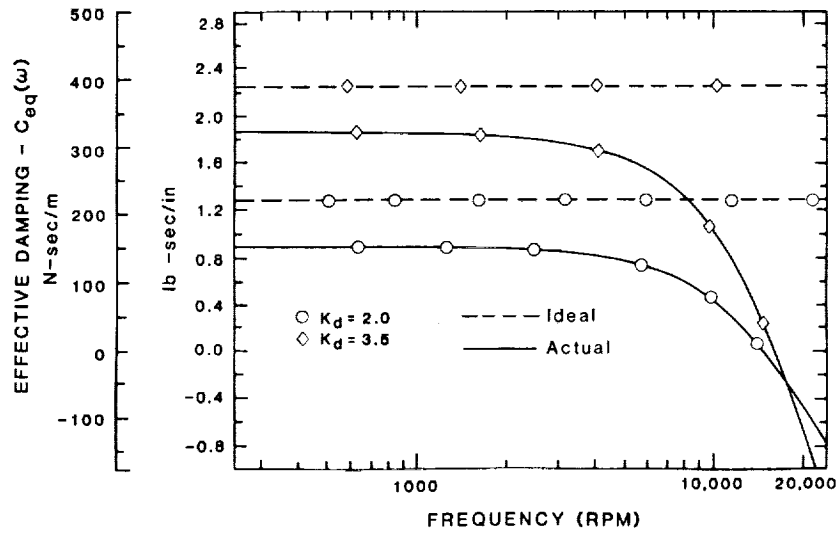


(B)

Figures 10A & 10B - $K_{eq}(\omega)$ and $C_{eq}(\omega)$
Varying Proportional Feedback (Digital)



(A)



(B)

Figures 11A & 11B - $K_{eq}(\omega)$ and $C_{eq}(\omega)$
Varying Derivative Feedback (Digital)

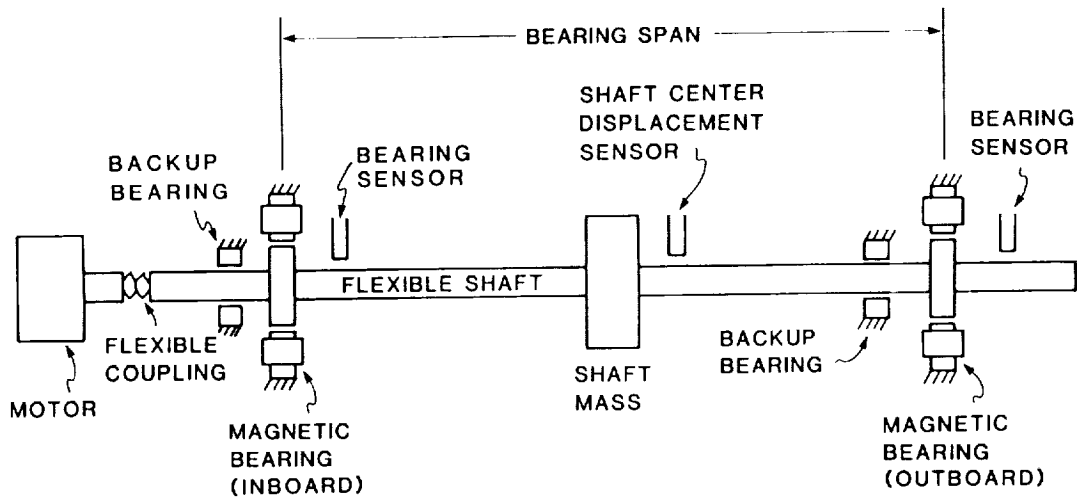


Figure 12 - Experimental Apparatus

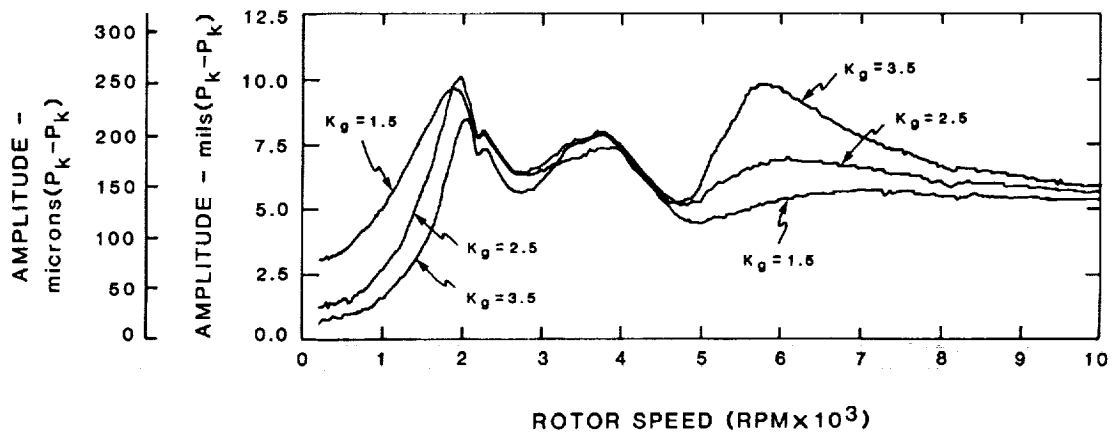


Figure 13A - Bearing Vertical Displacement - Varying Proportional Feedback (Analog Controller)

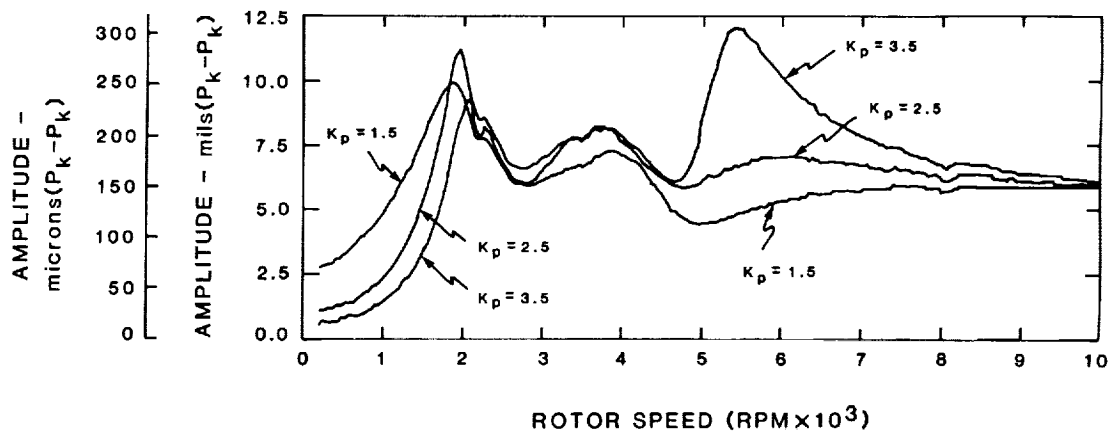


Figure 13B - Bearing Vertical Displacement - Varying Proportional Feedback (Digital Controller)

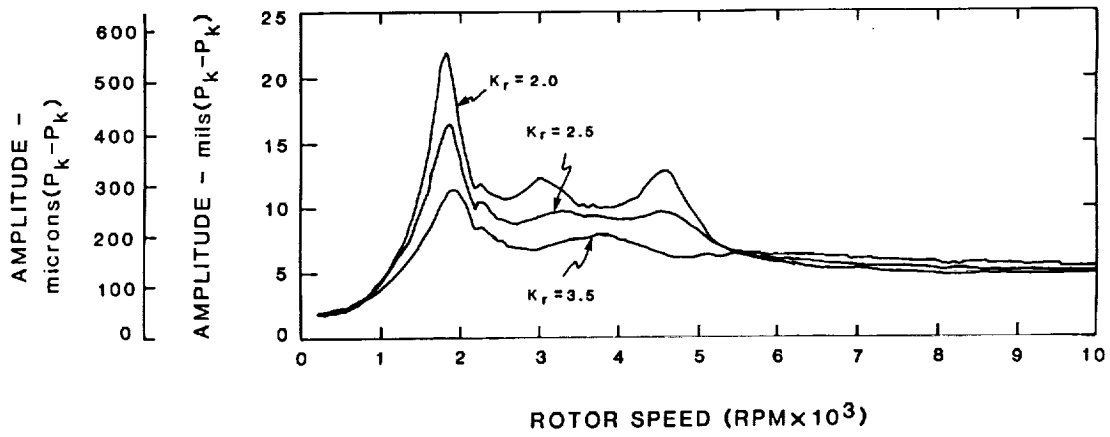


Figure 14A - Bearing Vertical Displacement - Varying Derivative Feedback (Analog Controller)

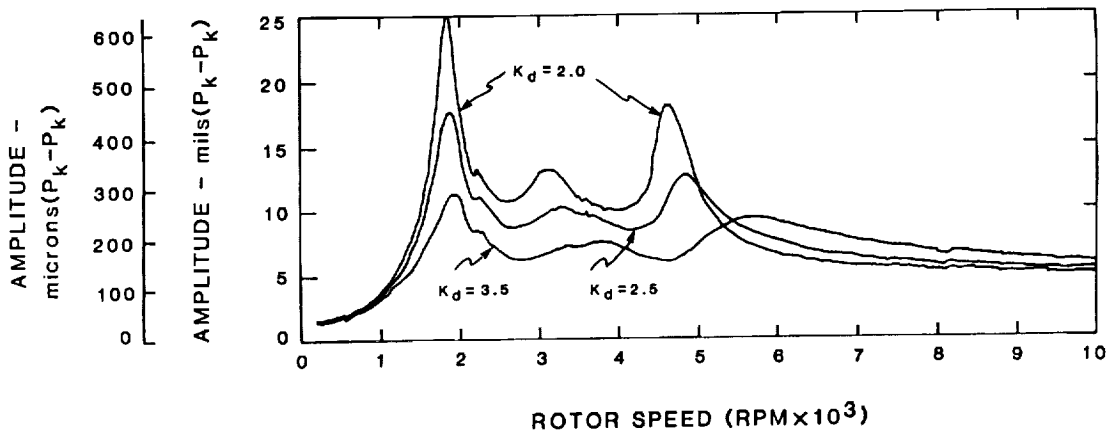


Figure 14B - Bearing Vertical Displacement - Varying Derivative Feedback (Digital Controller)

